RESEARCH ARTICLE

Structural and Functional Adaptation of Vancomycin Resistance VanT Serine Racemases

Djalal Meziane-Cherif,[a] Peter J. Stogios,[b,c] Elena Evdokimova,[b,c] Olga Egorova,[b,c] Alexei Savchenko,[b,c] Patrice Courvalin[a]

Institut Pasteur, Unité des Agents Antibactériens, Paris, France[a]; Department of Chemical Engineering and Applied Chemistry, University of Toronto, Toronto, Ontario, Canada[b]; Center for Structural Genomics of Infectious Diseases (CSGID)[c]

D.M.-C. and P.J.S. contributed equally to this work.

ABSTRACT **Vancomycin resistance in Gram-positive bacteria results from the replacement of the D-alanyl–D-alanine target of peptidoglycan precursors with D-alanyl–D-lactate or D-alanyl–D-serine (D-Ala-D-Ser), to which vancomycin has low binding affinity. VanT is one of the proteins required for the production of D-Ala-D-Ser-terminating precursors by converting L-Ser to D-Ser. VanT is composed of two domains, an N-terminal membrane-bound domain, likely involved in L-Ser uptake, and a C-terminal cytoplasmic catalytic domain which is related to bacterial alanine racemases. To gain insight into the molecular function of VanT, the crystal structure of the catalytic domain of $VanT_G$ from VanG-type resistant *Enterococcus faecalis* BM4518 was determined. The structure showed significant similarity to type III pyridoxal 5′-phosphate (PLP)-dependent alanine racemases, which are essential for peptidoglycan synthesis. Comparative structural analysis between $VanT_G$ and alanine racemases as well as site-directed mutagenesis identified three specific active site positions centered around Asn_{696} which are responsible for the L-amino acid specificity. This analysis also suggested that VanT racemases evolved from regular alanine racemases by acquiring additional selectivity toward serine while preserving that for alanine. The 4-fold-lower relative catalytic efficiency of $VanT_G$ against L-Ser versus L-Ala implied that this enzyme relies on its membrane-bound domain for L-Ser transport to increase the overall rate of D-Ser production. These findings illustrate how vancomycin pressure selected for molecular adaptation of a housekeeping enzyme to a bifunctional enzyme to allow for peptidoglycan remodeling, a strategy increasingly observed in antibiotic-resistant bacteria.**

IMPORTANCE **Vancomycin is one of the drugs of last resort against Gram-positive antibiotic-resistant pathogens. However, bacteria have evolved a sophisticated mechanism which remodels the drug target, the D-alanine ending precursors in cell wall synthesis, into precursors terminating with D-lactate or D-serine, to which vancomycin has less affinity. D-Ser is synthesized by VanT serine racemase, which has two unusual characteristics: (i) it is one of the few serine racemases identified in bacteria and (ii) it contains a membrane-bound domain involved in L-Ser uptake. The structure of the catalytic domain of $VanT_G$ showed high similarity to alanine racemases, and we identified three specific active site substitutions responsible for L-Ser specificity. The data provide the molecular basis for VanT evolution to a bifunctional enzyme coordinating both transport and racemization. Our findings also illustrate the evolution of the essential alanine racemase into a vancomycin resistance enzyme in response to antibiotic pressure.**

Received 13 May 2015 **Accepted** 2 July 2015 **Published** 11 August 2015

Citation Meziane-Cherif D, Stogios PJ, Evdokimova E, Egorova O, Savchenko A, Courvalin P. 2015. Structural and functional adaptation of vancomycin resistance VanT serine racemases. mBio 6(4):e00806-15. doi:10.1128/mBio.00806-15.

Invited Editor Gilles P. van Wezel, Leiden University **Editor** Gerard D. Wright, McMaster University

Address correspondence to Patrice Courvalin, pcourval@pasteur.fr, or Alexei Savchenko, alexei.savchenko@utoronto.ca..

Glycopeptides, such as vancomycin and teicoplanin, are key agents for the treatment of infections caused by antibiotic-resistant Gram-positive bacteria, but widespread clinical resistance to these drugs has become a major public health problem (1). Vancomycin blocks bacterial cell wall synthesis by binding the D-alanyl–D-alanine (D-Ala-D-Ala) C-terminal dipeptide of the muramyl pentapeptide moiety of peptidoglycan precursors, thereby interfering with the transglycosylase and transpeptidase activities of penicillin-binding proteins (PBPs) (2). Resistance arises from the ability of bacteria to produce modified peptidoglycan precursors ending in D-alanyl–D-lactate (D-Ala-D-Lac) or D-alanyl–D-serine (D-Ala-D-Ser), to which glycopeptides exhibit weak affinity (3). Nine vancomycin resistance (*van*) gene clusters have been described in enterococci and have been distinguished according to their specificities to incorporate either D-Ala-D-Lac (VanA, VanB, VanD, and VanM) or D-Ala-D-Ser (VanC, VanG, VanE, VanL, and VanN) in late precursors (3–6).

Synthesis of the D-Ala-D-Ser dipeptide requires two proteins: VanT, a membrane-bound racemase that converts L-Ser into D-Ser, and a ligase (VanC, VanG, VanE, VanL, and VanN) that links D-Ser to D-Ala (7). The pool of vancomycin-susceptible precursors is reduced by the hydrolysis of the D-Ala terminating dipeptide and pentapeptide species by the D,D-dipeptidase/D,D-pentapeptidase VanXY (8).

Serine racemases are mainly found in mammals, where D-Ser acts as a modulator of brain function (9, 10). In prokaryotes, this activity appears to be present primarily in glycopeptide-resistant Gram-positive bacteria (11). The VanT racemase was first characterized in a VanC-type-resistant *Enterococcus gallinarum* isolate (4, 11–13). The $vanT_C$ gene encodes a 698-amino-acid polypeptide containing an N-terminal (residues 1 to 322) membrane-bound domain that belongs to the acyltransferase superfamily (Pfam clan CL0316) whose role is attributed to L-Ser transport (4), and a C-terminal (residues 323 to 698) cytoplasmic domain where the catalytic activity is located (11, 13). This domain architecture is conserved among the $VanT_E$, $VanT_G$, and $VanT_N$ representatives (14–16) but differs in the *vanL* gene cluster (5), where two separate genes, $vanT_{mL}$ and $vanT_{rL}$, encode, respectively, the membrane-bound and the cytosolic domains, implying that these two functionalities are required for resistance. The C-terminal domain of $VanT_C$ is 25% identical in sequence with *Enterococcus faecalis* alanine rasemase (*Ef*Alr) (17) and conserves the pyridoxal 5′-phosphate (PLP) attachment motif present in the Alr protein. This domain functions as an Alr as it interconverts L-Ala and D-Ala, although this activity is 6-fold lower than that toward L-Ser (13). Alrs belong to the type III class of PLP-dependent enzymes (10) based on their structural arrangement (17–20). All characterized members of this enzyme family are homodimeric, with the two protomers associated in a head-to-tail fashion. Each subunit displays an N-terminal $(\alpha/\beta)_8$/TIM barrel domain and a C-terminal β-barrel fold domain. The active site is located in a cleft between the two domains at the dimer interface, where the PLP cofactor is tethered as an internal aldimine (Schiff base) with the ε-amino group of a catalytic lysine.

Alrs are highly specific for alanine racemization, and structure-function studies have led to a generally accepted reaction mechanism which involves a lysine and a tyrosine acting as acid-base catalysts for, respectively, donating and abstracting an α-hydrogen from the bound isomer of the substrate, D-Ala or L-Ala (20–22). In the L → D catalytic conversion, the L-Ala substrate first displaces the lysine and forms with PLP an L-external aldimine, which is then deprotonated by the tyrosine from the other subunit to produce an unstable carbanion. This carbanion is then reprotonated on the opposite face by the lysine to generate a D-external aldimine with PLP. The final step is the loss of the D-Ala product by transamination, and this recycles the internal lysine L-aldimine (20). These two key catalytic residues are conserved between Alrs and VanT enzymes (11), suggesting that the mechanism for racemization of serine is similar to that of alanine.

While this comparative analysis provided insights into the general reaction catalyzed by VanT enzymes, the molecular basis of their specificity toward L-Ser has not been investigated in detail. A study of the Alr from *Bacillus stearothermophilus* (*Bs*Alr) suggested that the highly conserved Tyr_{354} is a key determinant for alanine specificity (23). Its replacement with an asparagine, which occupies the corresponding position in VanT enzymes, led to a 62-fold increase in serine racemase activity with no significant change in alanine racemization (23). However, no VanT enzyme has been structurally characterized, limiting our understanding of the molecular function of this unique serine racemase family and its role in vancomycin resistance.

In this study, we determined the crystal structure of the $VanT_G$ catalytic domain and studied the role of active site residues in catalysis and specificity by site-directed mutagenesis. Our data provide the molecular basis of the altered specificity of VanT toward L-Ser and provide clues as to the possible route of evolution of this resistance-related activity from that of common alanine racemases.

TABLE 1 $VanT_G$ crystal X-ray diffraction data collection and refinement statistics

Parameter	Data
Diffraction data	
Space group	$P2_1$
Cell dimensions	
a, *b*, *c* (Å)	78.7, 82.3, 117.5
β (°)	90.1
Resolution (Å)	20.0–2.00
R_{sym}[a]	0.112 (0.547)
$I/\sigma(I)$	16.8 (2.86)
Completeness (%)	100 (100)
Redundancy	7.7 (6.8)
Refinement statistics	
Resolution (Å)	19.9–2.02
No. of reflections (working, test)	97,095, 1,871
R factor/free R factor[b]	18.2/23.3 (33.1/37.3)
No. of refined atoms	
Protein (no. of molecules)	11,591 (4)
Solvent	28
Water	700
B factors	
Protein	35.2
Solvent	28.9
Water	35.8
RMSD of:	
Bond lengths (Å)	0.007
Bond angles (°)	1.037

[a] R_{sym} is the symmetry-related reflection statistic as used in reference 47; in parentheses is the value for the outer shell of data.
[b] R factor defined as in reference 47; the values in parentheses are for the outer shells of the data.

RESULTS

$VanT_G$ structure, active site, and comparison with Alrs. In order to determine the structure of VanT enzymes, we expressed and purified the cytoplasmic domains of the VanT proteins from the *vanC*, *vanG*, *vanL*, and *vanN* vancomycin resistance operons. We successfully crystallized the $VanT_G$ domain encompassing residues 339 to 712 and determined its structure by the single anomalous dispersion (SAD) method to a resolution of 2.02 Å using a selenomethionine-derivatized protein crystal (Table 1).

The crystal structure of $VanT_G$ revealed four protein chains arranged into two almost-identical homodimers which superimposed with a root mean square deviation (RMSD) of 0.6 Å across equivalent Cα atoms (their entire chains), and thus we focused our analysis on the "AB" dimer. The subunits for each $VanT_G$ dimer interacted in a "head-to-tail" fashion and displayed an N-terminal $(\alpha/\beta)_8$/TIM barrel and a C-terminal 9-stranded β-barrel. Both domains in the $VanT_G$ subunit contributed to the dimerization interface, which covered 2,615 $Å^2$ and involved over 75 amino acids from each subunit (Fig. 1A). This extensive nature of the dimerization interface is consistent with the predominantly dimeric nature of $VanT_G$ in solution, as determined by size exclusion chromatography (data not shown). The structure showed significant similarity with that of *Ef*Alr (17), *Bs*Alr (20), and *Vibrio cholerae* Alr (*Vc*Alr) (Fig. 1B). A structural homology search also

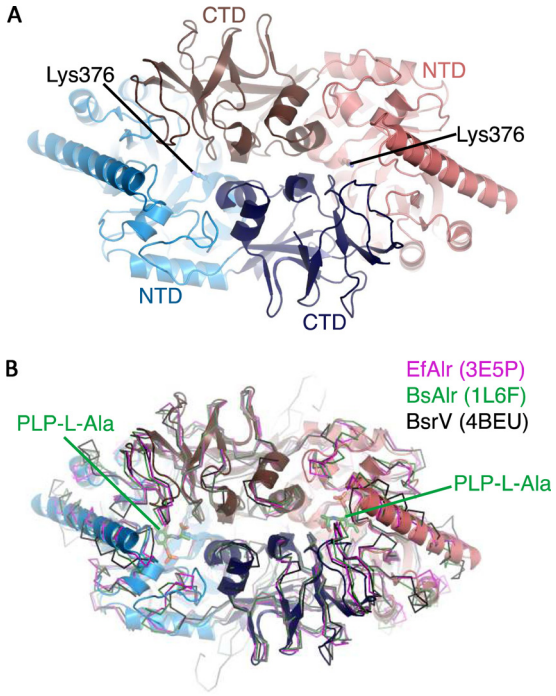

FIG 1 Structure of $VanT_G$. (A) Homodimer of $VanT_G$, showing the head-to-tail arrangement. One subunit (red and brown) contains the $(\alpha/\beta)_8$/TIM barrel domain at the N terminus (red) and the β-strands domain at the C terminus (brown). The PLP-binding site is indicated by the conserved Lys376 in the N-terminus. (B) Superposition of the $VanT_G$ homodimer colored as for panel A with various alanine racemase homologues shown in a ribbon diagram. The PLP cofactor bound to L-Ala in the *Bs*Alr structure is shown as green sticks.

revealed that $VanT_G$ is similar to other structurally characterized racemases, such as the broad-spectrum racemase BsrV and Bar from, respectively, *V. cholerae* (24) (Fig. 1B) and *Pseudomonas putida* (25), and to the lysine racemase Lyr from *Proteus mirabilis* (25). This analysis also confirmed that $VanT_G$ is a member of the type III PLP-dependent class of enzymes with significant overall structural similarity to specific and nonspecific amino acid racemases.

Multiple-sequence alignment of Alr, broad-spectrum, lysine-specific, and VanT racemases indicated that all these enzymes share active site residues (Fig. 2). However, a phylogenetic reconstruction differentiated three distinct groups according to amino acid specificity, with Lyr grouping with the broad-spectrum racemases (Fig. 2). This analysis indicated that while these enzymes share an overall structural architecture, they clearly contain distinct sequence signatures that correlate with their substrate specificity.

As with previously characterized racemase enzymes, the $VanT_G$ active site is located at the interface between the N-terminal TIM barrel and the C-terminal β-barrel domain at the bottom of a deep, positively charged pocket (see Fig. S1 in the supplemental material). We did not observe electron density consistent with the presence of PLP in any active site of the $VanT_G$ structure, based on a close analysis of the simulated annealing omit map (see Fig. S2 in the supplemental material). We experimented with modeling of PLP bound in an aldimine bond with each of the Lys_{376} residues; however, crystallographic refinement of this model resulted in negative density features surrounding multiple cofactor atoms, including the presumptive aldimine bond. Alternatively, refinement of the occupancy of the cofactor resulted in only insignificant occupancy values (no greater than 0.29, as in the chain C active site). Therefore, we were confident that our crystallographic data were best represented by one sulfate and multiple water molecules in each active site rather than the presence of the PLP cofactor. Crystallization of $VanT_G$ in the presence of excess PLP also did not result in determination of a PLP-bound $VanT_G$ structure. However, the superposition of the PLP-bound *Bs*Alr (PDB 1L6F) and $VanT_G$ structures showed a high level of structural congruence between the PLP-coordinating and active site residues (Fig. 3). The superposition did not reveal any significant steric clashes between the PLP molecule and $VanT_G$ active site residues, suggesting that the position of PLP is conserved in these enzymes. This alignment indicated that the $VanT_G$ residues which are likely involved in PLP binding include Lys_{376}, Tyr_{380}, Arg_{470}, His_{498}, Gly_{559}, Val_{560}, and Tyr_{622}' (where $'$ designates the residue from the other $VanT_G$ subunit). Notably, each of these residues is conserved between all Alr and VanT homologs, except for Val_{560}, which is replaced by either an Ile or a Gly (Fig. 2). The hydrogen-bonding network in the $VanT_G$ active site involving the backbone amides of Tyr_{622}' and Met_{652}' and two water molecules was spatially identical to a similar network in *Bs*Alr involving Tyr_{284}' and Met_{312}', a water molecule, and the carboxylate of the amino acid substrate (Fig. 3). The lysine/tyrosine acid-base pair (Lys_{39} and Tyr_{265}) in *Bs*Alr corresponded to $VanT_G$ residues Lys_{376} and Tyr_{603}, and this pair is also conserved in other VanT enzymes (Fig. 2). However, the position of Tyr_{603} in $VanT_G$ was different from that of Tyr_{265} in *Bs*Alr, likely due to the lack of PLP bound to $VanT_G$, which led to the change in conformation of the loop carrying this catalytic residue (Fig. 3).

Taken together, these observations indicated significant structural similarities between VanT and Alr enzymes which extend into the catalytic site, and from these we expect that both enzyme groups rely on the same catalytic mechanism. The degree of similarity also implied that the distinct amino acid specificity of these enzyme groups could be structurally rationalized.

Role of critical residues in serine selectivity. Kinetic analysis demonstrated that $VanT_G$ possesses racemase activity against both L-Ala and L-Ser substrates (Fig. 4A; see also Table S2 in the supplemental material) and is 4-fold more efficient in converting L-Ala than L-Ser, based on the k_{cat}/K_m ratios (Fig. 4B). The catalytic efficiency of $VanT_G$ against L-Ala was similar to that of *Vc*Alr (24) but much less than that of *Bs*Alr (23).

To gain deeper insight into the structural elements responsible for $VanT_G$ activity against L-Ser, we analyzed the differences between active sites of $VanT_G$ and of the strict L-Ala racemase *Bs*Alr. The $VanT_G$ active site contained 4 amino acids (Tyr_{543}, Ser_{567}, Thr_{695}, and Asn_{696}) that formed a hydrogen-bonded network not observed in the *Bs*Alr enzyme which was due to a change in the conformation of the loop containing Ser_{567} (Fig. 3). Importantly, Asn_{696} was positioned within 3.5 Å of the methyl group of PLP–L-Ala bound to *Bs*Alr. A model of L-Ser at this position showed its side chain hydroxyl within 2.9 Å of Asn_{696} (Fig. 3); therefore, this residue would be appropriately positioned to interact with the serine substrate. Furthermore, in $VanT_G$, the Asn_{696} and Ser_{567} residues form hydrogen bonds with a water molecule that may assist in coordination of PLP, since it occupies the same position as *Bs*Alr Tyr_{354}, whose hydroxyl interacts with the PLP phosphate group. All four positions were conserved within, but not between,

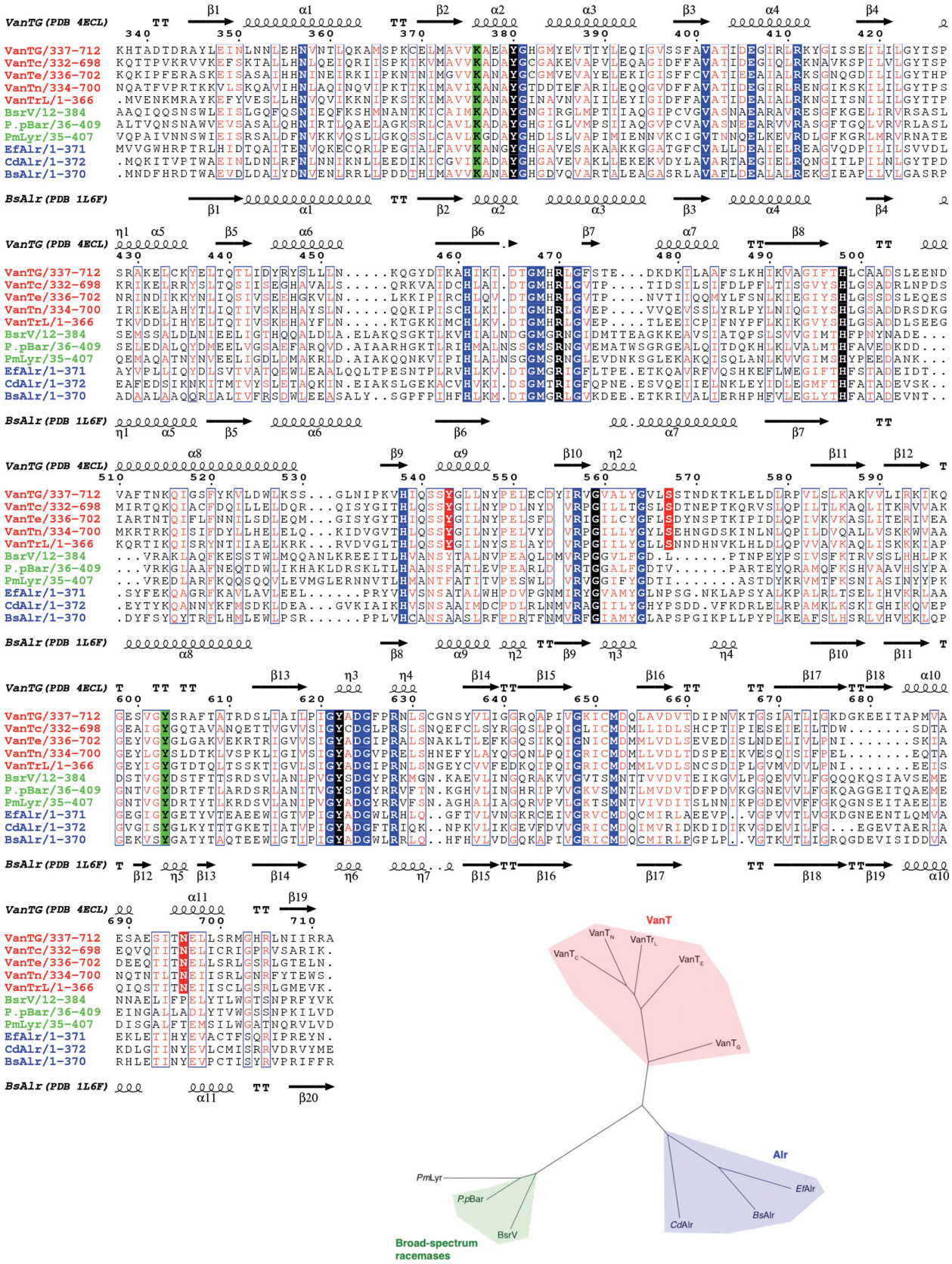

FIG 2 Sequence relationships of bacterial amino acid racemases. (Top) Multiple-sequence alignment of VanTs, Alrs, and broad-spectrum racemases. $VanT_G$ was aligned with VanT racemases (red) from *van* operons ($VanT_C$, $VanT_E$, $VanT_N$, and $VanT_{rL}$), broad-spectrum racemases (green) (*V. cholerae* BsrV, *P. putida* *(Continued)*

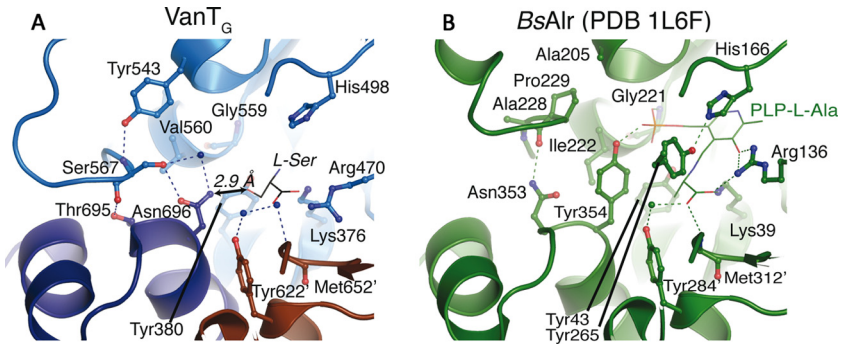

FIG 3 Comparison of VanT$_G$ (A) and *Bs*Alr (B) active sites. Active site residues are shown by sticks. The PLP-binding site in VanT$_G$ is shown in blue, and the adjacent monomer is brown. L-Ser, shown as stick lines, was modeled by manual placement onto the coordinates of L-Ala from PLP-Ala in the *Bs*Alr structure (green). Water molecules are indicated as spheres.

the VanT and Alr classes (i.e., Tyr-Ser-Thr-Asn in VanT enzymes and Ala-Pro-His/Asn-Tyr in Alr enzymes), suggesting that they play key but different roles in their respective enzyme classes (Fig. 2).

Based on this information, we probed the VanT-specific active site residues Tyr$_{543}$, Ser$_{567}$, Thr$_{695}$, and Asn$_{696}$ by site-directed mutagenesis to elucidate their contributions to substrate selectivity. We constructed 13 VanT$_G$ variants by replacing these residues with their equivalents in *Bs*Alr and tested them for their ability to catalyze the conversion of L-Ala and L-Ser (see Table S2 in the supplemental material).

The kinetic parameters of the VanT$_G$ Tyr$_{543}$Ala and Thr$_{695}$Ser mutants were similar to those of the wild-type enzyme (Fig. 4A; see also Table S2 in the supplemental material). This indicated that a single alteration in the hydrogen bonds formed by these residues is not sufficient to affect VanT$_G$ racemase activity or substrate selectivity. In contrast, the Ser$_{567}$Pro mutation led to a significant decrease in both racemase activities, affecting the K_m and k_{cat} values for L-Ala and L-Ser conversion (Fig. 4A; see also Table S2); the corresponding catalytic efficiencies dropped 12- and 8-fold, respectively. Since the serine/alanine racemase efficiency ratio for this VanT$_G$ variant did not change significantly, 2.7 versus 4.4 for the wild type (Fig. 4B), it is likely that the observed effect is due to destabilization of the active site. In support of this notion, the combination of Ser$_{567}$Pro with the Tyr$_{543}$Ala substitution had a less detrimental effect on the enzyme's activity, while the Tyr$_{543}$Ala/Ser$_{567}$Pro double mutant retained significant activity against L-Ala and L-Ser (Fig. 4A; see also Table S2). The latter substitution would provide the space necessary to accommodate the larger proline side chain. These results indicated that, although Tyr$_{543}$, Thr$_{695}$, and Ser$_{567}$ active site residues are conserved among VanT enzymes (Fig. 2), they have no direct effect on the substrate specificity of VanT$_G$.

The remaining VanT-specific active site residue VanT$_G$ Asn$_{696}$ corresponded to Tyr$_{354}$ in *Bs*Alr. The mutation Asn$_{696}$Ala did not have a strong effect on the catalytic efficiency against either L-Ala or L-Ser. This substitution reduced the k_{cat} values for L-Ala and L-Ser conversion by 3- and 4-fold, respectively, but this effect was offset by corresponding 3- and 4-fold drops in K_m values (see Table S2 in the supplemental material). In sharp contrast, the Asn$_{696}$Tyr substitution resulted in a 30-fold drop in L-Ser conversion without affecting the enzyme's activity against L-Ala, leading to an increase of the alanine/serine racemase efficiency ratio up to 217 (Fig. 4B). Importantly, the K_m value for the activity of the Asn$_{696}$Tyr mutant against L-Ser increased 5-fold and that for L-Ala decreased 4-fold (see Table S2). These observations indicated that Asn$_{696}$ is critical to confer VanT$_G$ substrate selectivity and that a tyrosine substitution at this position likely obstructs the binding of the larger side chain of the L-Ser substrate.

We thus postulated that the effect of the Asn$_{696}$Tyr mutation on VanT$_G$ activity against L-Ala can be offset by additional mutations that would allow for full recovery of the activity against this substrate. This strategy could have been adopted in Alr, and thus additional mutations may effectively convert VanT$_G$ into an alanine racemase. To test this hypothesis, we generated the VanT$_G$ double mutants Tyr$_{543}$Ala/Asn$_{696}$Tyr and Ser$_{567}$Pro/Asn$_{696}$Tyr and the triple mutant Tyr$_{543}$Ala/Ser$_{567}$Pro/Asn$_{696}$Tyr. Kinetic analysis of these variants showed that the two double mutants had higher alanine/serine efficiency ratios than the wild-type enzyme (65 and 128, respectively, versus 4.4 for the wild type). These values, however, were much lower than that of the Asn$_{696}$Tyr mutant (217) (Fig. 4B). The fact that the Ser$_{567}$Pro/Asn$_{696}$Tyr double mutation increased serine racemase activity to an extent lower than Asn$_{696}$Tyr could reflect the decrease in conformational flexibility necessary for accommodating the larger tyrosine residue caused by the Ser$_{567}$Pro replacement. Strikingly, the triple Tyr$_{543}$Ala/Ser$_{567}$Pro/Asn$_{696}$Tyr mutant was severely compromised in serine racemase activity, with a 7-fold increase in the K_m and an 11-fold drop in the k_{cat} value for L-Ser (see Table S2 in the supplemental material). In contrast, the activity of this mutant against L-Ala was less affected and showed a 4-fold change in both the K_m and k_{cat} values. The catalytic efficiency of the triple mutant for L-Ser con-

Figure Legend Continued

Bar, and *P. mirabilis* PmLyr), and Alrs homologues (blue) (*E. faecalis* Alr, *C. difficile* Alr, and *B. stearothermophilus* Alr). The numbering above the sequences corresponds to that of VanT$_G$. Secondary elements from VanT$_G$ and *Bs*Alr structures are shown, respectively, above and below the primary sequences. Conserved amino acids are shown in blue, those of the PLP-binding site are in black, and those responsible for VanT specificity are red. The key Lys/Tyr acid-base pair for the abstraction/donation of the α-hydrogen is indicated in green. The figure was generated with ESPript 3.0 (bottom). Phylogenetic reconstruction of the aligned racemases was performed using the maximum likelihood algorithm in the MEGA package and visualized with FigTree.

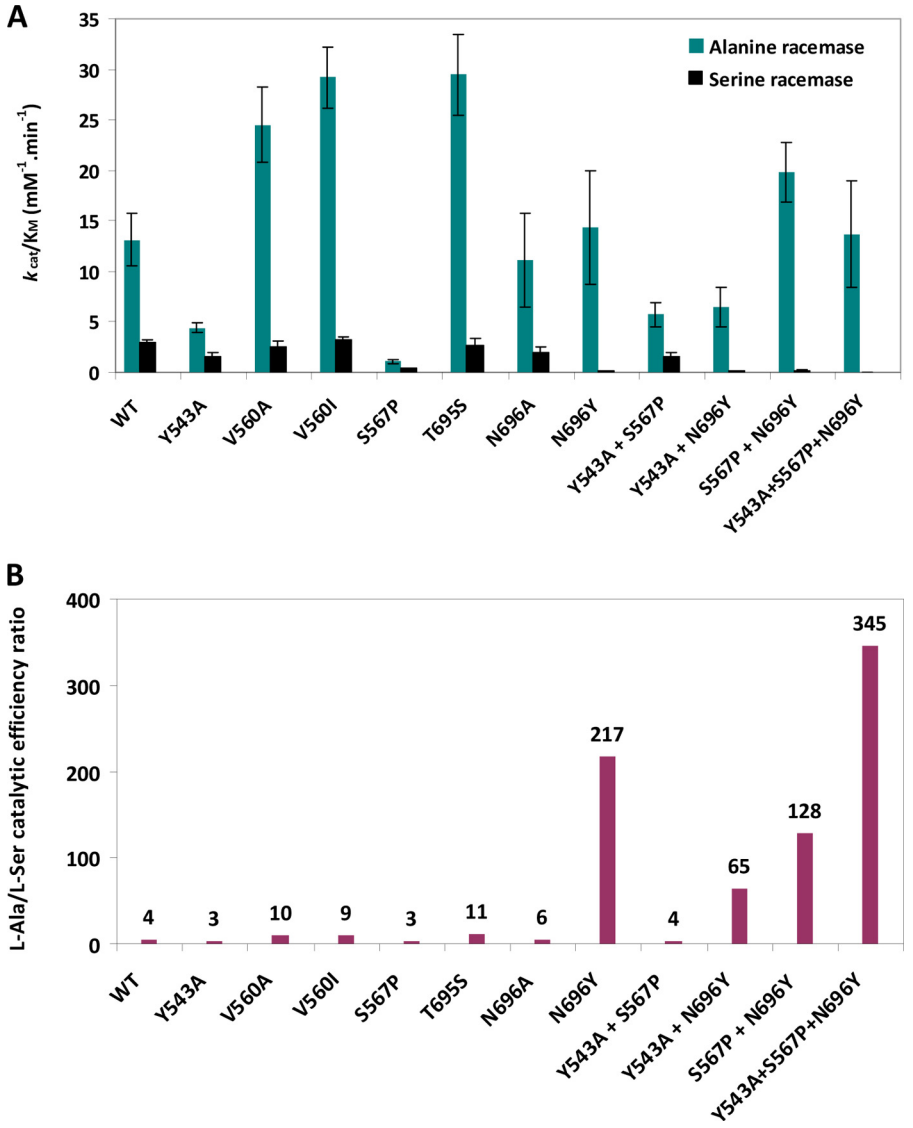

FIG 4 Comparison of alanine and serine racemase activities of $VanT_G$ mutants. (A) Catalytic efficiencies of alanine and serine racemase activities. Detailed kinetic parameters (mean values of at least three independent measurements) are indicated in Table S2 in the supplemental material. (B) L-Ala/ L-Ser catalytic efficiency ratios. Values are indicated on top of the bars.

version was severely reduced and 75-fold lower than that of the wild type. This $VanT_G$ variant demonstrated a catalytic efficiency for L-Ala conversion comparable to that of the wild type, and thus its alanine/serine racemase activity ratio was the highest observed, 345, in the variants (Fig. 4B). Combined, our data point to Asn_{696} as the key residue for $VanT_G$ serine racemase specificity and that substitution of its chemical environment by the *Bs*Alr equivalents, as shown by analysis of the triple $Tyr_{543}Ala/Ser_{567}Pro/Asn_{696}Tyr$ mutant, resulted in nearly complete conversion of $VanT_G$ into a strict alanine racemase.

DISCUSSION

Bacteria use D-amino acids, commonly D-Ala and D-Glu, as building blocks for their peptidoglycan layer, and this isomer is thought to provide resistance to most proteases. Emerging evidence suggests that D-amino acids regulate cell wall remodeling and strength (26) and can affect biofilm formation and stability (27). Amino acid racemases, which convert the natural L-amino acids to their D-counterparts, play important roles in bacterial biology. They are classified as PLP-dependent and -independent enzymes which follow two distinct reaction mechanisms (10). Among the PLP-dependent group, the alanine racemases (Alrs) are ubiquitous and essential for growth of bacteria but are absent in mammals, which makes them attractive targets for antimicrobials. Consequently, Alrs have been extensively studied for their reaction chemistry and three-dimensional structure, providing a good understanding of their molecular mechanism (17, 19, 20). In contrast, PLP-dependent serine racemases are very rare in bacteria and, to the best of our knowledge, the only known role of these enzymes is for incorporation of D-Ser in the peptidoglycan of vancomycin-resistant bacteria (28). Broad-spectrum racemases, including BsrV from *V. cholerae*, produce D-Ser (24), but the biological role

of this D-amino acid is unknown. The VanT vancomycin resistance serine racemases are similar to Alrs (11), suggesting that these proteins could be derived from the same ancestor. Yet, VanTs are distinct from Alr based on the presence of an atypical membrane-bound domain that is presumably involved in L-Ser transport (4).

As the role of D-Ser in vancomycin resistance has been clearly established, we were interested in elucidating the molecular basis and the evolution of VanT specificity. We thus determined the crystal structure of the $VanT_G$ C-terminal catalytic domain. The structure showed significant overall similarity with those of Alrs from *B. stearothermophilus* (20) and *E. faecalis* (17). We took advantage of this homology to probe the active site of $VanT_G$ by using site-directed mutagenesis.

Analysis of the $VanT_G$ and *Bs*Alr structures supports the notion that VanT and Alr have a common ancestor (11). The evolution in substrate specificity was clearly dependent on substitution of residues at key positions of the active site surrounding the substrate amino acid side chain. Mutagenesis pointed to the crucial role of the conserved $VanT_G$ Asn_{696} in serine recognition. Replacement of this residue by a tyrosine, which would mimic the active site in Alrs, decreased the ability of $VanT_G$ for L-Ser conversion by 30-fold without affecting alanine racemase activity. This result is in agreement with the finding that the reverse mutation, $Tyr_{354}Asn$, in *Bs*Alr increases serine racemase activity by 62-fold (23). However, in contrast to this study, where *Bs*Alr $Tyr_{354}Asn$ had a relatively minor effect on the K_m for L-Ser, the K_m value of the $VanT_G$ $Asn_{696}Tyr$ mutant for L-Ser was 5-fold higher than that of the wild type. Thus, $Asn_{696}Tyr$ in $VanT_G$ is likely to cause steric hindrance to the binding of L-Ser. Since the turnover of L-Ser by the $Asn_{696}Tyr$ mutant was decreased by 3-fold, asparagine at this position must play an indirect role in catalysis, perhaps by stabilizing the carbanion intermediate through a hydrogen bond to the serine hydroxyl side chain; this possibility is consistent with the modeling of L-Ser into the active site of $VanT_G$ structure and the analysis of the *Bs*Alr $Tyr_{354}Asn$ mutant (23).

Mutagenesis also highlighted the role of $VanT_G$ active site residues proximal to Asn_{696}. The steric hindrance imposed by Tyr_{696} was less pronounced in the double mutants (see Table S2 in the supplemental material); the additional mutations might provide space necessary to accommodate Tyr_{696}. The $VanT_G$ triple mutant ($Tyr_{543}Ala/Ser_{567}Pro/Asn_{696}Tyr$) demonstrated almost exclusive alanine racemase activity, consistent with the hypothesis that the hydrogen-bonding network of Tyr_{543}, Ser_{567}, Thr_{695}, and Asn_{696} positions the Asn_{696} amide appropriately for interaction with the L-Ser hydroxyl group.

The importance of this area of the active site of racemases in determining amino acid specificity is supported by the recent discovery of broad-spectrum amino acid racemases (24). A comparison of BsrV, which is active against 10 amino acids, with $VanT_G$ indicated that the PLP-coordinating residues are conserved while the 4 amino acids that were subjected to mutagenesis in $VanT_G$ are not (Fig. 2); specifically, $VanT_G$ Asn_{696} was equivalent to Pro_{391} in BsrV. Such variation may lead to a more accessible active site in BsrV compared to Alr or $VanT_G$, resulting in broader specificity. Similarly, the Bar and Lyr L-lysine-specific racemases had smaller amino acids (alanine and threonine, respectively) at the same position, enabling these enzymes to accommodate the longer lysine side chain. These observations are in further support of the relevance of this area of the racemase active sites for specificity.

Many antibiotic resistance enzymes can be traced back to primary "housekeeping" functions in bacterial biology, and the current understanding suggests that mutations, gene duplications, or overexpression of essential genes can provide new or extended specificities. This "proto-resistance" concept (29) is supported by the evolution of several antibiotic resistance enzymes, such as the β-lactamases (30) and RND efflux systems (31). We have shown that such a phenomenon occurred in the evolution of the VanXY vancomycin resistance D,D-dipeptidase/D,D-pentapeptidase. This enzyme is related in sequence and structure to members of the M15B peptidase family, which includes D-Ala-D-Ala-containing pentapeptide-specific hydrolases (8). VanY, a D-Ala-D-Ala-specific pentapeptidase, evolved into VanXY through acquisition of the "bisubstrate loop," which added hydrolysis of D-Ala-D-Ala to that of a D-Ala-D-Ala-containing pentapeptide. Furthermore, this adaptive functionality is specific: VanXY is not active against the dipeptide and pentapeptide ending in D-Ser, provided by the molecular architecture of the active site. $VanT_G$ followed a similar evolutionary path: it retained activity against L-Ala but acquired additional specificity toward L-Ser due to the active site modifications centered around Asn_{696}.

Replacement of a preexisting strict alanine racemase by a strict serine racemase would appear more efficient to confer resistance rather than evolution to an enzyme with both specificities. However, given that $VanT_G$ retains alanine racemase activity, the mutations acquired by a VanT-Alr progenitor were probably insufficient to evolve with a strict serine racemase. This could result from the fact that, even with the presence of Asn_{696}, the active site of $VanT_G$ can still accommodate the smaller L-Ala. Thus, VanT enzymes have evolved by expanding, rather than switching, their substrate specificity compared to their VanT-Alr progenitors.

Given the dual specificity of $VanT_G$ and its relatively low activity toward L-Ser, it is likely that fusion of the racemase domain with a membrane-bound acyltransferase which imports L-Ser provides improved racemization and thus better adaptation for vancomycin resistance. Fusion of two genes with complementary functions is a strategy for antibiotic resistance evolution, which has been increasingly observed and results in extremely broad-spectrum resistance (32). It also has the advantage of gene coexpression, which reduces the biological cost associated with resistance (33). The most striking example is the bifunctional AAC(6′)/APH(2″) in Gram-positive cocci, which combines two aminoglycoside-modifying activities, acetylation and phosphorylation, with complementary substrate profiles as separate domains of a single protein (34). Of note, all the VanT racemases, except that of VanL-type resistance, resulted from gene fusion and have evolved as bifunctional enzymes (5). In VanL, the two functions are encoded by separate and adjacent genes; this likely represents an intermediate step in evolution. Apparently, this strategy was an efficient alternative to further specification of a racemase active site to an L-Ser substrate which, as already mentioned, might not be possible due to the smaller L-Ala side chain that could still be accommodated in the L-Ser-binding site.

Overall, this detailed structural and functional analysis of $VanT_G$ reinforces the notion that antibiotic resistance arises from preexisting housekeeping enzymes via acquisition of genetic changes that lead to expanded specificity or higher activity. The selective pressure of antibiotics can also select for the emergence and spread of bifunctional enzymes, and VanT racemases provide

a prime example for a sophisticated evolution that has combined both strategies.

MATERIALS AND METHODS

Cloning and mutagenesis. The C-terminal portion of *vanT*$_G$ (encoding amino acids 339 to 712) was amplified from *E. faecalis* BM4518 genomic DNA by PCR and cloned into p15Tv-LIC (35), which provided an N-terminal His$_6$ tag fusion followed by a tobacco etch virus (TEV) protease cleavage site between the tag and residue 339 of VanT$_G$. Mutations in *vanT*$_G$ were introduced by using the QuikChange mutagenesis kit (Stratagene) with oligonucleotide pairs (see Table S1 in the supplemental material).

Protein expression and purification. The N-terminal His$_6$-tagged wild-type and mutant VanT$_G$ proteins were produced in *E. coli* BL21-CodonPlus(DE3)-RIPL (Novagen) harboring the corresponding hybrid plasmid. Freshly transformed cells were grown in 0.5 liters of LB medium containing 25 μg/ml of chloramphenicol and 100 μg/ml of ampicillin. The culture was incubated at 37°C to an optical density at 600 nm of 0.8, at which point it was induced for 16 h at 16°C with 1 mM isopropyl-1-thio-β-D-galactopyranoside. For structural analysis, selenomethionine-substituted *vanT*$_G$ was expressed using the standard M9 high-yield growth procedure according to the manufacturer's (Shanghai Medicilon) instructions and *E. coli* BL21(DE3)-CodonPlus. Cells were harvested by centrifugation and resuspended in 20 ml of buffer A (50 mM HEPES [pH 7.5], 300 mM NaCl, 10% [vol/vol] glycerol) supplemented with 10% (vol/vol) BugBuster 10× protein extraction reagent (Novagen), 25 units of Benzonase (Sigma-Aldrich), and 5 mM imidazole. The mixture was stirred for 10 min at room temperature and centrifuged at 20,000 × *g* for 45 min, and the supernatant was applied to a 1-ml HisTrap Fast Flow column (GE Healthcare, Uppsala, Sweden) equilibrated with buffer A containing 40 mM imidazole. The protein was eluted using buffer A with a gradient of 40 to 500 mM imidazole over 20 ml. For structural analysis, the His$_6$ tag was removed by cleavage with TEV protease overnight at 4°C in dialysis buffer containing 0.3 M NaCl, 50 mM HEPES (pH 7.5), 5% glycerol, and 0.5 mM tris(2-carboxyethyl)phosphine, followed by binding to a HisTrap Fast Flow column and capture of the flowthrough. Fractions containing the VanT$_G$ proteins were identified by SDS-PAGE, pooled, and dialyzed overnight against 50 mM HEPES (pH 7.5), 300 mM NaCl, 5% (vol/vol) glycerol, and 1 mM Tris(2-carboxyethyl)phosphine, concentrated when needed with a Centriprep 30 concentrator, and stored at −80°C.

Kinetic analysis. Determination of Ala and Ser racemase activities of VanT$_G$ proteins was based on the amino acid oxidase-lactate dehydrogenase (LDH)-coupled assay (36). The reaction was carried out in a 0.1-ml total volume containing 50 mM HEPES (pH 8.0), 0.2 mM NADH, 0.01 μg of LDH, 0.03 μg of D-amino acid oxidase (D-AAO), 100 units of catalase at 37°C, 15 μg of VanT$_G$ enzyme, and various concentrations of L-Ala or L-Ser. VanT$_G$ converts L-Ala and L-Ser into D-Ala and D-Ser, respectively. D-AAO converts D-Ala and D-Ser into, respectively, pyruvate and 3-hydroxypyruvate, which are reduced by LDH. The consumption of NADH, reflected in the formation of L-lactate or 2,3-dihydroxypropane, was followed at 340 nm. The steady-state kinetic parameters (mean values of at least three independent measurements) were obtained by fitting experimental data to the Hanes-Woolf equation (37) using the program EnzFitter (Biosoft, Cambridge, United Kingdom).

Crystallization and structure determination. Selenomethionine-derivatized VanT$_G$ (residues 339 to 712) was crystallized at room temperature by the hanging drop method with 1 μl of a 23-mg/ml protein solution mixed with 1 μl of reservoir solution (0.2 M ammonium sulfate, 0.2 M sodium chloride, 0.1 M morpholineethanesulfonic acid [pH 6.5], and 30% [wt/vol] polyethylene glycol monomethyl ether 5000). This crystal was cryoprotected with paratone oil in a liquid nitrogen stream before data collection. Diffraction data at 100 K were collected at the Advanced Photon Source (APS), Argonne National Laboratory, Life Sciences Collaborative Access Team beamline 21-ID-G fitted with a MarMosaic 300 charge-coupled device at the selenium absorption peak (0.97856 Å). X-ray data were reduced with HKL-3000 (38). The VanT$_G$ structure was solved by SAD phasing using Phenix.autosol (39), which identified 27 of the 28 selenium sites in the asymmetric unit (four protein chains, each with seven selenomethionine residues). An initial model of the protein was built using Phenix.autobuild followed by rounds of manual model building and refinement with Coot (40) and Phenix.refine. Isotropic B-factors were refined with translation-libration-screw motion (TLS) parameterization (TLS groups were residues 340 to 582 and residues 583 to 711 for each protein chain). To obtain a bias-free model view of the VanT$_G$ active sites, we generated a simulated annealing omit map by deleting all active site residues, ions, and water molecules shown in Fig. 3 as well as all atoms within 5 Å of these groups, followed by simulated annealing using the Phenix.refine algorithm (default parameters). The resulting F_O-F_C map was inspected with Coot (40). The final VanT$_G$ model included residues 340 to 711 of four protein chains forming two homodimers. Average B-factor and bond angle/length RMSD values were calculated using Phenix. All geometry was verified using the Phenix and Coot validation tools plus the PDB Adit server. The VanT$_G$ structure had a good backbone with the following percentages of residues in the most favored, additional allowed, generously allowed, and disallowed regions, respectively, of the Ramachandran plot: 90.8%, 8.9%, 0.2%, and 0%.

Structural analysis. Structure similarity searches were performed using the PDBeFold server (41, 42). Structure superpositions and analysis were performed with PyMOL (43). L-Ser was modeled in the active site of VanT$_G$ by manual placement onto the coordinates of L-Ala from PLP–L-Ala in *B. stearothermophilus* Alr (PDB 1L6F) (20). The side chain rotamer of L-Ser was the *m* rotamer (χ_1 angle = −65°).

Sequence alignment and phylogenetic reconstruction. Sequences of VanT, Alr, and broad-spectrum and lysine racemases were aligned using Clustal Omega (44) and visualized with the ESPript 3 server (http://espript.ibcp.fr) (45). Phylogenetic reconstruction was performed using the maximum likelihood algorithm in the MEGA package (46) and visualized with FigTree (http://tree.bio.ed.ac.uk/software/figtree).

Protein structure accession number. The VanT$_G$ structure has been deposited in the Protein Databank under the accession code 4ECL.

SUPPLEMENTAL MATERIAL

Supplemental material for this article may be found at http://mbio.asm.org/lookup/suppl/doi:10.1128/mBio.00806-15/-/DCSupplemental.

Figure S1, TIF file, 1.1 MB.
Figure S2, TIF file, 1.8 MB.
Table S1, DOC file, 0.03 MB.
Table S2, DOC file, 0.1 MB.

ACKNOWLEDGMENTS

We thank R. Di Leo for technical assistance and Z. Wawrzak at the Life Sciences Collaborative Access Team/Advanced Photon Source for X-ray data collection.

This project has been funded in whole or in part with federal funds from the National Institute of Allergy and Infectious Diseases, National Institutes of Health, Department of Health and Human Services (contracts HHSN272200700058C and HHSN272201200026C) and by an unrestricted grant from Reckitt Benckiser.

REFERENCES

1. **Butler MS, Hansford KA, Blaskovich MA, Halai R, Cooper MA.** 2014. Glycopeptide antibiotics: back to the future. J Antibiot (Tokyo) **67:** 631–644. http://dx.doi.org/10.1038/ja.2014.111.
2. **Reynolds PE.** 1989. Structure, biochemistry and mechanism of action of glycopeptide antibiotics. Eur J Clin Microbiol Infect Dis **8:**943–950. http://dx.doi.org/10.1007/BF01967563.
3. **Courvalin P.** 2006. Vancomycin resistance in gram-positive cocci. Clin Infect Dis **42**(Suppl 1):S25–S34. http://dx.doi.org/10.1086/491711.
4. **Arias CA, Peña J, Panesso D, Reynolds P.** 2003. Role of the transmembrane domain of the VanT serine racemase in resistance to vancomycin in

Enterococcus gallinarum BM4174. J Antimicrob Chemother **51:**557–564. http://dx.doi.org/10.1093/jac/dkg128.

5. **Boyd DA, Willey BM, Fawcett D, Gillani N, Mulvey MR.** 2008. Molecular characterization of Enterococcus faecalis N06-0364 with low-level vancomycin resistance harboring a novel D-Ala-D-Ser gene cluster, vanL. Antimicrob Agents Chemother **52:**2667–2672. http://dx.doi.org/10.1128/AAC.01516-07.
6. **Wu D, Zhang L, Kong Y, Du J, Chen S, Chen J, Ding J, Jiang H, Shen X.** 2008. Enzymatic characterization and crystal structure analysis of the D-alanine–D-alanine ligase from *Helicobacter pylori*. Proteins **72:** 1148–1160. http://dx.doi.org/10.1002/prot.22009.
7. **Meziane-Cherif D, Saul FA, Haouz A, Courvalin P.** 2012. Structural and functional characterization of VanG D-Ala:D-Ser ligase associated with vancomycin resistance in Enterococcus faecalis. J Biol Chem **287:** 37583–37592. http://dx.doi.org/10.1074/jbc.M112.405522.
8. **Meziane-Cherif D, Stogios PJ, Evdokimova E, Savchenko A, Courvalin P.** 2014. Structural basis for the evolution of vancomycin resistance D,D-peptidases. Proc Natl Acad Sci U S A **111:**5872–5877. http://dx.doi.org/10.1073/pnas.1402259111.
9. **Yoshimura T, Goto M.** 2008. D-Amino acids in the brain: structure and function of pyridoxal phosphate-dependent amino acid racemases. FEBS J **275:**3527–3537. http://dx.doi.org/10.1111/j.1742-4658.2008.06516.x.
10. **Conti P, Tamborini L, Pinto A, Blondel A, Minoprio P, Mozzarelli A, De Micheli C.** 2011. Drug discovery targeting amino acid racemases. Chem Rev **111:**6919–6946. http://dx.doi.org/10.1021/cr2000702.
11. **Arias CA, Martín-Martinez M, Blundell TL, Arthur M, Courvalin P, Reynolds PE.** 1999. Characterization and modelling of VanT: a novel, membrane-bound, serine racemase from vancomycin-resistant *Enterococcus gallinarum* BM4174. Mol Microbiol **31:**1653–1664. http://dx.doi.org/10.1046/j.1365-2958.1999.01294.x.
12. **Arias CA, Courvalin P, Reynolds PE.** 2000. *vanC* cluster of vancomycin-resistant *Enterococcus gallinarum* BM4174. Antimicrob Agents Chemother **44:**1660–1666. http://dx.doi.org/10.1128/AAC.44.6.1660-1666.2000.
13. **Arias CA, Weisner J, Blackburn JM, Reynolds PE.** 2000. Serine and alanine racemase activities of VanT: a protein necessary for vancomycin resistance in *Enterococcus gallinarum* BM4174. Microbiology **146:** 1727–1734.
14. **Abadía Patiño L, Courvalin P, Perichon B.** 2002. *vanE* gene cluster of vancomycin-resistant *Enterococcus faecalis* BM4405. J Bacteriol **184:** 6457–6464. http://dx.doi.org/10.1128/JB.184.23.6457-6464.2002.
15. **Depardieu F, Bonora MG, Reynolds PE, Courvalin P.** 2003. The vanG glycopeptide resistance operon from Enterococcus faecalis revisited. Mol Microbiol **50:**931–948. http://dx.doi.org/10.1046/j.1365-2958.2003.03737.x.
16. **Lebreton F, Depardieu F, Bourdon N, Fines-Guyon M, Berger P, Camiade S, Leclercq R, Courvalin P, Cattoir V.** 2011. D-Ala-D-Ser VanN-type transferable vancomycin resistance in Enterococcus faecium. Antimicrob Agents Chemother **55:**4606–4612. http://dx.doi.org/10.1128/AAC.00714-11.
17. **Priyadarshi A, Lee EH, Sung MW, Nam KH, Lee WH, Kim EE, Hwang KY.** 2009. Structural insights into the alanine racemase from Enterococcus faecalis. Biochim Biophys Acta **1794:**1030–1040. http://dx.doi.org/10.1016/j.bbapap.2009.03.006.
18. **Couñago RM, Davlieva M, Strych U, Hill RE, Krause KL.** 2009. Biochemical and structural characterization of alanine racemase from Bacillus anthracis (Ames). BMC Struct Biol **9:**53. http://dx.doi.org/10.1186/1472-6807-9-53.
19. **Asojo OA, Nelson SK, Mootien S, Lee Y, Rezende WC, Hyman DA, Matsumoto MM, Reiling S, Kelleher A, Ledizet M, Koski RA, Anthony KG.** 2014. Structural and biochemical analyses of alanine racemase from the multidrug-resistant Clostridium difficile strain 630. Acta Crystallogr D Biol Crystallogr **70:**1922–1933. http://dx.doi.org/10.1107/S1399004714009419.
20. **Watanabe A, Yoshimura T, Mikami B, Hayashi H, Kagamiyama H, Esaki N.** 2002. Reaction mechanism of alanine racemase from Bacillus stearothermophilus: X-ray crystallographic studies of the enzyme bound with N-(5′-phosphopyridoxyl)alanine. J Biol Chem **277:**19166–19172. http://dx.doi.org/10.1074/jbc.M201615200.
21. **Watanabe A, Yoshimura T, Mikami B, Esaki N.** 1999. Tyrosine 265 of alanine racemase serves as a base abstracting alpha-hydrogen from L-alanine: the counterpart residue to lysine 39 specific to D-alanine. J Biochem **126:**781–786. http://dx.doi.org/10.1093/oxfordjournals.jbchem.a022517.
22. **Watanabe A, Kurokawa Y, Yoshimura T, Kurihara T, Soda K, Esaki N, Watababe A.** 1999. Role of lysine 39 of alanine racemase from Bacillus stearothermophilus that binds pyridoxal 5′-phosphate. Chemical rescue studies of Lys39 → Ala mutant. J Biol Chem **274:**4189–4194. http://dx.doi.org/10.1074/jbc.274.7.4189.
23. **Patrick WM, Weisner J, Blackburn JM.** 2002. Site-directed mutagenesis of Tyr354 in Geobacillus stearothermophilus alanine racemase identifies a role in controlling substrate specificity and a possible role in the evolution of antibiotic resistance. Chembiochem **3:**789–792. http://dx.doi.org/10.1002/1439-7633(20020802)3:8<789::AID-CBIC789>3.0.CO;2-D.
24. **Espaillat A, Carrasco-López C, Bernardo-García N, Pietrosemoli N, Otero LH, Álvarez L, de Pedro MA, Pazos F, Davis BM, Waldor MK, Hermoso JA, Cava F.** 2014. Structural basis for the broad specificity of a new family of amino-acid racemases. Acta Crystallogr D Biol Crystallogr **70:**79–90. http://dx.doi.org/10.1107/S1399004713024838.
25. **Wu HM, Kuan YC, Chu CH, Hsu WH, Wang WC.** 2012. Crystal structures of lysine-preferred racemases, the non-antibiotic selectable markers for transgenic plants. PLoS One **7:**e48301. http://dx.doi.org/10.1371/journal.pone.0048301.
26. **Cava F, Lam H, de Pedro MA, Waldor MK.** 2011. Emerging knowledge of regulatory roles of D-amino acids in bacteria. Cell Mol Life Sci **68:** 817–831. http://dx.doi.org/10.1007/s00018-010-0571-8.
27. **Kolodkin-Gal I, Romero D, Cao S, Clardy J, Kolter R, Losick R.** 2010. D-Amino acids trigger biofilm disassembly. Science **328:**627–629. http://dx.doi.org/10.1126/science.1188628.
28. **Reynolds PE, Courvalin P.** 2005. Vancomycin resistance in enterococci due to synthesis of precursors terminating in D-alanyl-D-serine. Antimicrob Agents Chemother **49:**21–25. http://dx.doi.org/10.1128/AAC.49.1.21-25.2005.
29. **Morar M, Wright GD.** 2010. The genomic enzymology of antibiotic resistance. Annu Rev Genet **44:**25–51. http://dx.doi.org/10.1146/annurev-genet-102209-163517.
30. **Hall BG, Barlow M.** 2004. Evolution of the serine beta-lactamases: past, present and future. Drug Resist Updat **7:**111–123. http://dx.doi.org/10.1016/j.drup.2004.02.003.
31. **Yoon EJ, Courvalin P, Grillot-Courvalin C.** 2013. RND-type efflux pumps in multidrug-resistant clinical isolates of Acinetobacter baumannii: major role for AdeABC overexpression and AdeRS mutations. Antimicrob Agents Chemother **57:**2989–2995. http://dx.doi.org/10.1128/AAC.02556-12.
32. **Zhang W, Fisher JF, Mobashery S.** 2009. The bifunctional enzymes of antibiotic resistance. Curr Opin Microbiol **12:**505–511. http://dx.doi.org/10.1016/j.mib.2009.06.013.
33. **Foucault ML, Depardieu F, Courvalin P, Grillot-Courvalin C.** 2010. Inducible expression eliminates the fitness cost of vancomycin resistance in enterococci. Proc Natl Acad Sci U S A **107:**16964–16969. http://dx.doi.org/10.1073/pnas.1006855107.
34. **Ferretti JJ, Gilmore KS, Courvalin P.** 1986. Nucleotide sequence analysis of the gene specifying the bifunctional 6′-aminoglycoside acetyltransferase 2″ aminoglycoside phosphotransferase enzyme in Streptococcus faecalis and identification and cloning of gene regions specifying the two activities. J Bacteriol **167:**631–638.
35. **Eschenfeldt WH, Lucy S, Millard CS, Joachimiak A, Mark ID.** 2009. A family of LIC vectors for high-throughput cloning and purification of proteins. Methods Mol Biol **498:**105–115. http://dx.doi.org/10.1007/978-1-59745-196-3_7.
36. **Badet B, Roise D, Walsh CT.** 1984. Inactivation of the dadB Salmonella typhimurium alanine racemase by D and L isomers of beta-substituted alanines: kinetics, stoichiometry, active site peptide sequencing, and reaction mechanism. Biochemistry **23:**5188–5194. http://dx.doi.org/10.1021/bi00317a016.
37. **Henderson PJF.** 1992. Statistical analysis of enzyme kinetic data, p 277–313. In Eisenthal R, Danson MJ (ed), Enzyme assays, a practical approach. Oxford University Press, New York, NY.
38. **Minor W, Cymborowski M, Otwinowski Z, Chruszcz M.** 2006. HKL-3000: the integration of data reduction and structure solution—from diffraction images to an initial model in minutes. Acta Crystallogr D Biol Crystallogr **62:**859–866. http://dx.doi.org/10.1107/S0907444906019949.
39. **Adams PD, Afonine PV, Bunkóczi G, Chen VB, Davis IW, Echols N, Headd JJ, Hung LW, Kapral GJ, Grosse-Kunstleve RW, McCoy AJ, Moriarty NW, Oeffner R, Read RJ, Richardson DC, Richardson JS,**

Terwilliger TC, Zwart PH. 2010. PHENIX: a comprehensive python-based system for macromolecular structure solution. Acta Crystallogr D Biol Crystallogr **66:**213–221. http://dx.doi.org/10.1107/S0907444909052925.
40. **Emsley P, Cowtan K**. 2004. Coot: model-building tools for molecular graphics. Acta Crystallogr D Biol Crystallogr **60:**2126–2132. http://dx.doi.org/10.1107/S0907444904019158.
41. **Krissinel E, Henrick K**. 2004. Secondary-structure matching (SSM), a new tool for fast protein structure alignment in three dimensions. Acta Crystallogr D Biol Crystallogr **60:**2256–2268. http://dx.doi.org/10.1107/S0907444904026460.
42. **Holm L, Rosenström P**. 2010. Dali server: conservation mapping in 3D. Nucleic Acids Res **38:**W545–W549. http://dx.doi.org/10.1093/nar/gkq366.
43. **DeLano WL**. 2002. The PyMOL molecular graphics system. DeLano Scientific, Palo Alto, CA.
44. **Sievers F, Wilm A, Dineen D, Gibson TJ, Karplus K, Li W, Lopez R, McWilliam H, Remmert M, Söding J, Thompson JD, Higgins DG**. 2011. Fast, scalable generation of high-quality protein multiple sequence alignments using Clustal Ω. Mol Syst Biol **7:**539. http://dx.doi.org/10.1038/msb.2011.75.
45. **Robert X, Gouet P**. 2014. Deciphering key features in protein structures with the new ENDscript server. Nucleic Acids Res **42:**W320–W324. http://dx.doi.org/10.1093/nar/gku316.
46. **Tamura K, Peterson D, Peterson N, Stecher G, Nei M, Kumar S**. 2011. MEGA5: molecular evolutionary genetics analysis using maximum likelihood, evolutionary distance, and maximum parsimony methods. Mol Biol Evol **28:**2731–2739. http://dx.doi.org/10.1093/molbev/msr121.
47. **Cox G, Stogios PJ, Savchenko A, Wright GD**. 2014. Structural and molecular basis for resistance to aminoglycoside antibiotics by the adenylyltransferase ANT(2″)-Ia. mBio **6**(1)**:**e02180–14. http://dx.doi.org/10.1128/mBio.02180-14.